

Failure of curved brittle layer systems from radial cracking in concentrated surface loading

Matthew Rudas, Tarek Qasim, and Mark B. Bush
*School of Mechanical Engineering, The University of Western Australia, Crawley,
Western Australia 6009, Australia*

Brian R. Lawn^{a)}
*Materials Science and Engineering Laboratory, National Institute of Standards and Technology,
Gaithersburg, Maryland 20899-8500*

(Received 6 June 2005; accepted 14 July 2005)

A study was made of radial crack evolution in curved brittle layers on compliant support substrates. Three-dimensional boundary element analysis was used to compute the stepwise growth of radial cracks that initiate at the bottom surfaces of glass on polymeric support layers, from initiation to final failure. The algorithm calculates reconstituted displacement fields in the near-tip region of the extending cracks, enabling direct evaluation of stress-intensity factors. Available experimental data on the same material systems with prescribed surface curvatures were used to validate the essential features of the predicted crack evolution, particularly the stability conditions prior to ultimate failure. It was shown that the critical loads to failure diminish with increasing surface curvature. Generalization of the ensuing fracture mechanics to include alternative brittle-layer/polymer-substrate systems enabled an explicit expression for the critical load to failure in terms of material properties and layer thicknesses. Implications concerning practical layer systems, particularly dental crowns, are briefly discussed.

I. INTRODUCTION

Brittle layers on compliant substrates are relevant to a wide range of engineering coating and film applications. It has been well documented that radial cracks induced at brittle layer undersurfaces by contact-induced flexure are highly dangerous.¹⁻¹¹ A photograph of such a radial crack in a glass plate on a polycarbonate base is shown in Fig. 1.⁵ Such cracks form directly below the indentation center and propagate radially outward on median planes containing the indentation axis. Usually more than one such crack forms, in a regular star pattern. The crack fronts resemble contours of tensile hoop stresses in the flexing plate.¹²

In some layer systems, the surfaces may be curved, as in biomechanical structures like dental crowns on dentin^{13,14} or polyethylene-backed acetabular ceramic liners in total hip replacements,^{15,16} as well as in some coated tool and engine components. Whereas curvature may have little effect on the critical load to initiate radial cracks, it can have a considerable effect on the "failure" load to propagate these same cracks to the edges of the specimen.^{17,18} In crowns, the layers are basically (but not exclusively) convex, which can substantially exacerbate

unstable propagation. In acetabular cups, the articulating surface is concave, which tends to restrain crack extension.¹⁷ Other, top-surface, near-contact cracks can occur in brittle layer systems and may even dominate in some structures, especially in thicker brittle layers; such alternative crack systems have been adequately documented elsewhere and will not be considered in any detail here.^{19,20}

Indentation experiments conducted on brittle layer systems, specifically on ceramic slabs bonded to polymeric support substrates, show some distinctive features in radial crack evolution. The cracks initiate abruptly but then arrest. Initiation conditions have been well documented in flat-layer specimens, both experimentally and theoretically.^{5,7,9,11} To good approximation, initiation occurs when the tensile stress at the lower brittle surface exceeds the strength of the material. Once formed, the radial cracks propagate stably across the specimen with increasing load.¹² In flat and concave layers, this stability remains in effect until the cracks intersect the extreme edges of the specimen. In convex layers, the cracks break through to the upper surface after only limited propagation and then accelerate unstably to the specimen edges.¹⁷ The critical loads to produce this latter failure condition can be substantially higher than those for initiation, so there is a built-in damage tolerance. The mechanics of such failure are not so well understood. This is largely because geometry effects become exceedingly

^{a)}Address all correspondence to this author.

e-mail: brian.lawn@nist.gov
DOI: 10.1557/JMR.2005.0343

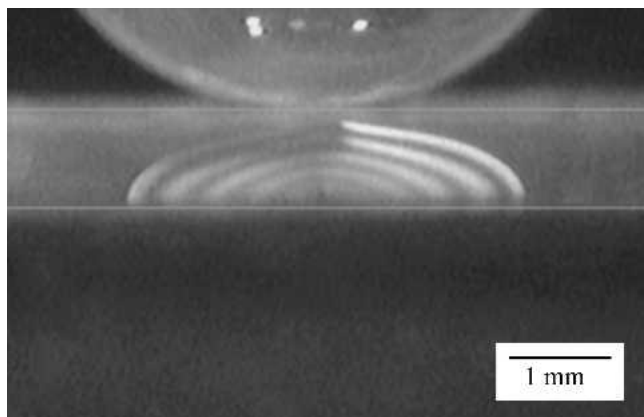


FIG. 1. Radial crack in glass 1 mm thick bonded to polycarbonate substrate. Indentation with WC sphere at load $P = 130$ N. Fizeau fringes from interface on loaded crack. (Top coating surface and coating/substrate interface artificially highlighted by white lines for clarity.) From Chai et al.⁵

complex once the radial crack dimension exceeds the layer thickness. One study of radial crack propagation in flat layers has been made using finite element analysis (FEA), but without any provision for ultimate failure.²¹ An attempt at an analytical fracture mechanics solution for the same system has also been conducted, but only with oversimplifying approximations (e.g., invariant penny-like geometry with total neglect of surface-interaction effects), and again without provision for failure.¹² No such attempt at all has been made for the more complex case of convex layer systems, where catastrophic failure is a major concern.

Accordingly, analysis of radial crack evolution in curved brittle layer systems forms the basis of the present study. The focus here is not so much on “crack prevention” as on “crack containment.”⁶ We use boundary element analysis (BEA) to calculate the stepwise growth of radial cracks from initiation to final failure.²² The BEA method calculates the reconstituted displacement field in the near-tip region of the extending crack, enabling direct evaluation of stress-intensity factors. Because the crack system is not axisymmetrical, three-dimensional (3D) analysis is required, adding to the complexity. The proposed analysis enables derivations of crack growth and ultimate failure relations. Comparison with experimental data for a model brittle bilayer material system—glass on epoxy—is used to validate essential predictions of the formulation.

II. NUMERICAL ANALYSIS OF CRACK EXTENSION: CASE STUDY ON CURVED GLASS/EPOXY BILAYERS

A. BEA computations

A schematic illustration of a curved brittle bilayer system containing a radial crack is shown in Fig. 2. A hard,

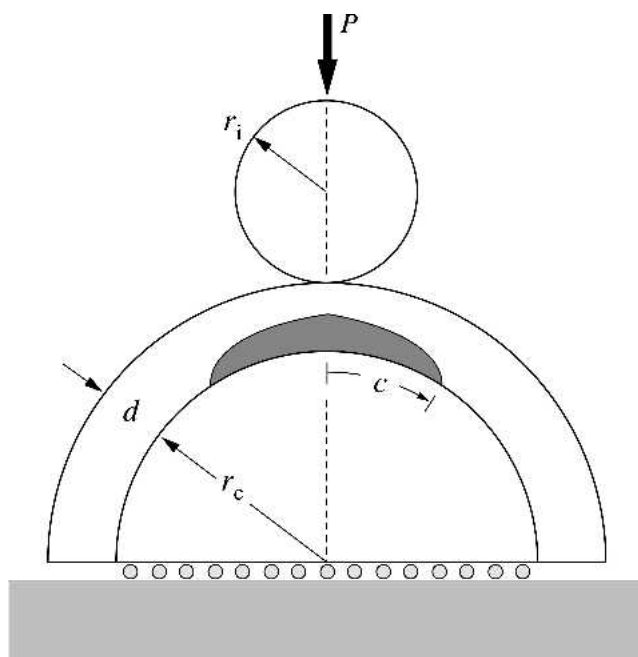


FIG. 2. Schematic illustration showing essential geometry of indenter contact on curved layer system containing radial crack (shaded).

frictionless indenter of radius r_i is loaded with normal axial force P onto a convex ceramic layer of thickness d and inner radius r_c filled with a compliant inner supporting material. The filler material is strongly bonded to the ceramic outer layer. The composite filled-ceramic structure is modeled as a hemisphere resting on a rigid plane. For simplicity, the ceramic layer does not make contact with this plane at its edges, i.e., unsupported margins, in approximate accordance with typical experimental conditions.¹⁷ One or more radial cracks form on median planes containing the load axis, with curvilinear dimension c measured along the inner circumference. These radial cracks are driven by hoop tensile stresses normal to the median planes. Although the cracks are not axisymmetric, they do have symmetry about the median planes, so extension occurs strictly in mode I. The object is to determine the evolution of the radial cracks from initial flaw through propagation to the specimen boundaries.

Boundary element analysis software (BEASY; Southampton, UK) is used to evaluate the crack system in Fig. 2.²³ Standard quadratic boundary elements are used and meshes configured with greatest concentration of elements around the critical crack tip regions, as shown in Fig. 3. Refinements in element density are made until the near-tip crack-wall displacement fields $u(x)$ (x = distance behind crack front) reach convergence. The familiar Irwin relation $K = u(\pi/8x)^{1/2}E_c/(1 - \nu_c^2)$, where E_c is Young's modulus and ν_c Poisson's ratio of the ceramic layer, provides the basis for computing the stress-intensity factor at any point along the crack front.²⁴

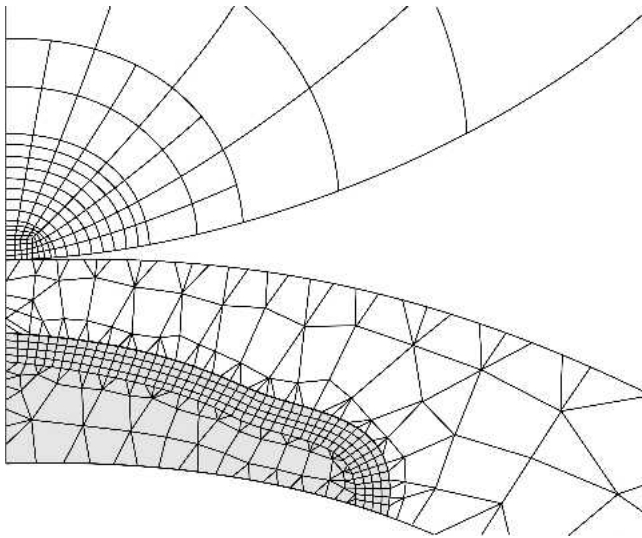


FIG. 3. Schematic illustration of mesh for crack in BEA calculations. Mesh is reconfigured with high density around the crack front at each extension increment.

BEA incrementing procedures used to follow the evolving crack geometries are subtle and will be outlined only briefly here, leaving fine details to be described elsewhere. The calculation begins with a small semicircular starting flaw of size c ($\ll d$) located directly below the contact at the bottom of the brittle layer. Contact is made at a specified load P and the stress-intensity factor K computed along the crack front. To allow for point-by-point variations in K , the crack shape is then adjusted according to $\delta\rho = \rho_0(\delta K/K_0)$, all the while holding c fixed at the bottom surface ($\rho =$ radial distance to front from crack center, ρ_0 and K_0 values at $\rho = c$, and $\delta K = K - K_0$). This process is repeated until the profile represents a front of equal K . Trial and error adjustments indicate that no more than two such iterations are required to achieve equi- K contours to within 5%. Then keeping load P fixed, the crack is incremented through Δc , with $\Delta\rho = \rho\Delta c/c$ to maintain the previous crack shape as a first approximation. The BEA mesh is then adapted to the new crack configuration, and the crack front adjusted to a constant K profile as before. This sequence is repeated until the crack extends to the extremities of the specimen.

Such a procedure enables determination of crack shapes and corresponding K fields at all stages in the evolution. We illustrate in the subsections below for a specific bilayer system, soda-lime glass layer on epoxy resin substrate, for which comparative experimental data are available.¹⁷ Input parameters for the BEA calculations are as follows: for glass, layer thickness $d = 1$ mm, Young's modulus $E_c = 70$ GPa, and Poisson's ratio $\nu_c = 0.22$; for epoxy, $E_s = 3.4$ GPa and $\nu_s = 0.33$; for indenter, $r_i = 4$ mm, $E_i = 614$ GPa, and $\nu_i = 0.22$ (tungsten carbide). While this choice of parameters is to

represent material systems that have been studied experimentally,¹⁷ we will assert a certain generality in the results.

B. Radial crack contours

Figure 4 shows the radial crack profile in our model flat layer system, superposed onto the experimentally observed profile in Fig. 1. The computed profile is chosen to match the measured base dimension of the observed crack. The basic profile of the observed crack is reproduced by the calculation. Note that this computed profile is far from the assumed penny-shaped profile of the originating small flaw, indicating that the crack is beginning to sense the presence of the top surface.

Sequential crack front profiles are plotted in Fig. 5 for various values of inner brittle plate radius r_c (Fig. 1). In all cases, the profile is relatively constrained in the vertical direction because of compression in the upper half of the flexing plate. This constraining effect becomes more evident as the crack expands into a more elongated geometry. Ultimately, at $c = c_B$, say, the radial crack intersects the top surface, here termed "breakthrough." Note that this breakthrough point occurs at smaller c_B for increasing curvature r_c^{-1} . Beyond the breakthrough point the crack straightens out into a near-linear front.

As indicated, these contours reproduce the main geometrical features of experimentally observed radial crack evolution. Examples of such penetrant cracks for flat and curved soda-lime layers on epoxy substrate are shown in Figs. 6 and 7, respectively. Straightening of the crack front beyond the breakthrough point is most apparent in the flat surface (Fig. 6). For the curved surface (Fig. 7), the straightened crack fronts persist to the base of the dome.

C. Crack evolution and critical loads for through-thickness penetration

The BEA algorithm is used to determine the loads P required to grow cracks of specific characteristic dimension c in the glass layers, by invoking the equilibrium condition that the stress-intensity factor K at the crack

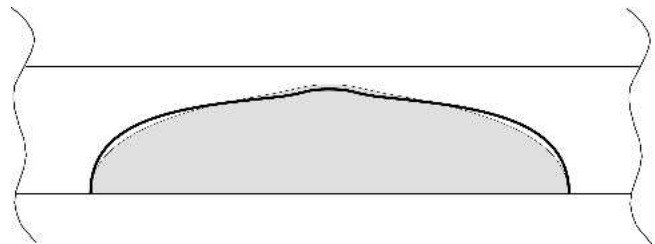


FIG. 4. Comparing shape of radial crack front from experiment from Fig. 1 (shaded) with BEA computation for a flat system consisting of glass plate of thickness 1 mm on polymer substrate (solid line). Contour is chosen to have same bottom-surface crack size as in experiment.

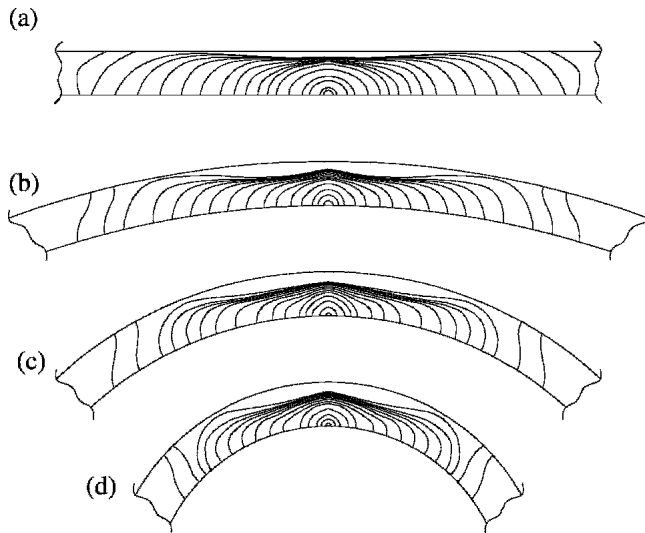
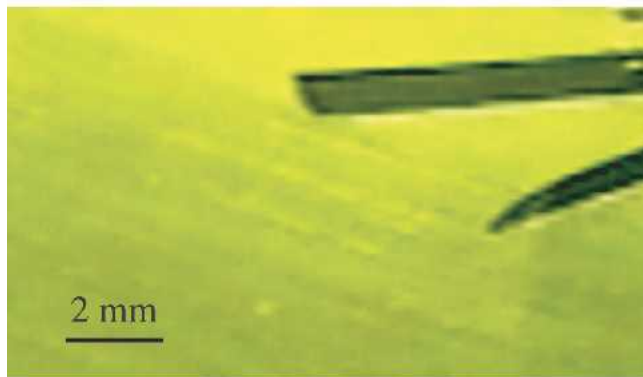


FIG. 5. Radial crack geometry evolution through brittle layers of different curvatures: (a) $r_c/d = \infty$ (flat), (b) $r_c/d = 20$, (c) $r_c/d = 8$, and (d) $r_c/d = 4$.



(a)



(b)

FIG. 6. Radial cracks in flat soda-lime glass layer of 1 mm thick epoxy resin substrate, indented with WC sphere of radius $r_i = 4$ mm at load $P = 1550$ N. Sequence showing radial cracks immediately (a) before and (b) after breakthrough. Glass undersurface abraded.

front should exceed the toughness K_c . Here we use a generic value of toughness $K_c = 1 \text{ MPa m}^{1/2}$, representative of a range of glasses and porcelains.^{11,25–27} We achieve the equilibrium configuration by first calculating

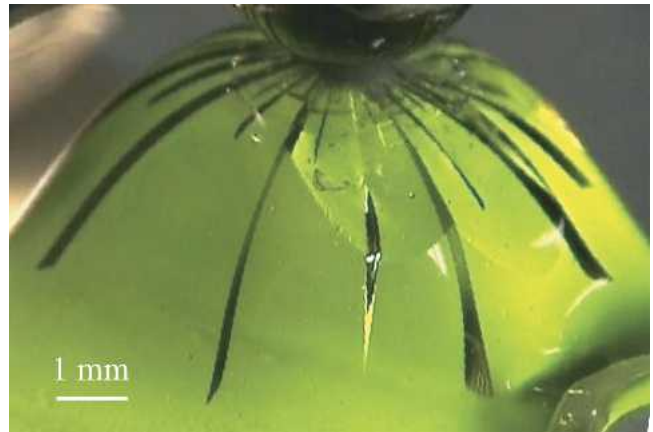


FIG. 7. Radial cracks in soda-lime glass layer of 1 mm thick and inner radius of curvature $r_c = 8$ mm on epoxy resin substrate, indented with WC sphere of radius $r_i = 4$ mm at load $P = 1500$ N. The glass undersurface is abraded. Straightened cracks extend to dome base.

K for a predetermined value of load P , as described in Sec. II. A, and then scaling K linearly with P while holding c constant until $K = K_c$. Repeat calculations for sequential incremental extensions Δc then enable determination of the equilibrium function $P(c)$.

Resulting functions are plotted in Fig. 8 as the smoothed solid curves for each prescribed inner glass plate radius r_c and thickness $d = 1$ mm. Corresponding experimental data from a preceding study for glass with abraded undersurfaces are included for comparison.¹⁷ The predicted $P(c)$ curves reproduce the broader trends in the data. These trends include the existence of at least one unstable branch ($dP/dc < 0$) and stable branch ($dP/dc > 0$) for all cases (i.e., all r_c). Arrows indicate instabilities in the crack propagation. Radial crack pop-in occurs from a small flaw on the first unstable branch ($c_f \approx 10 \mu\text{m}$ for abraded glass surfaces)⁵ to the adjacent stable branch. The popped-in cracks then propagate along the stable branch until, in the case of curved surfaces (finite r_c), the $P(c)$ curves pass through a maximum. As indicated in Sec. II. B (Fig. 5), this maximum corresponds closely to the breakthrough condition ($P = P_B$, $c = c_B$), at which point the cracks become unstable again. For the intermediate cases, $r_c = 8$ and 4 mm, the newly unstable cracks propagate to the edges of the specimen, whereas in the case $r_c = 20$ mm the unstable crack arrests once more in the long-crack region. The absence of any such maximum for flat surfaces ($r_c = \infty$) is consistent with a relatively high stability in the long-crack region for this limiting case.

Figure 9 plots the critical load P_B for radial crack breakthrough versus inverse plate inner radius r_c^{-1} for the glass/epoxy bilayers represented in Fig. 8. Figure 10 is the analogous plot of critical crack size c_B versus r_c^{-1} . The solid curves in these figures are the BEA predictions (envelopes of maxima in Fig. 8) and the data points are

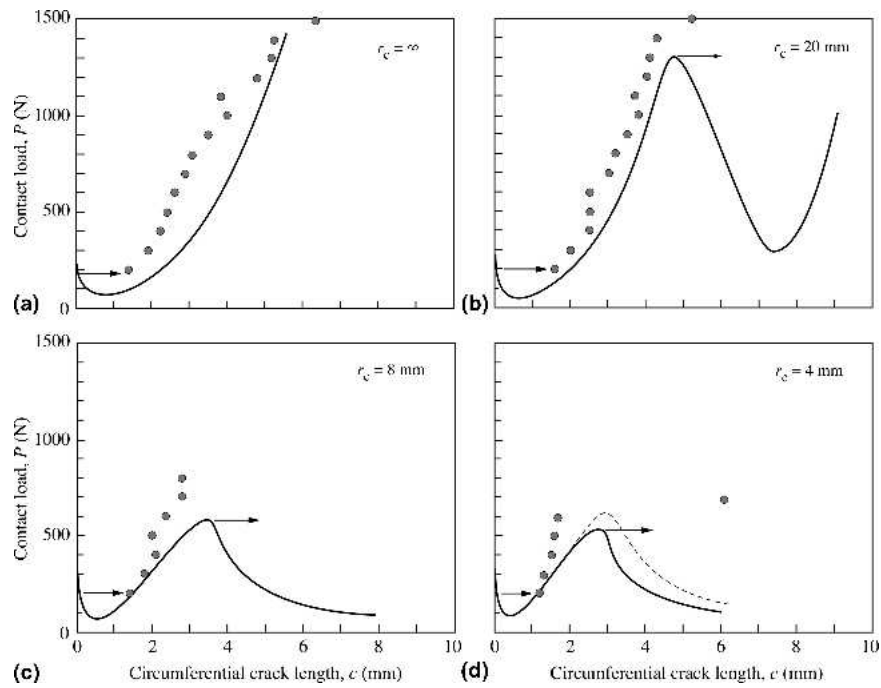


FIG. 8. Indentation load P versus radial crack size c for equilibrium extension conditions in glass layers $d = 1$ mm on epoxy support: (a) $r_c = \infty$, (b) $r_c = 20$ mm, (c) $r_c = 8$ mm, and (d) $r_c = 4$ mm. Solid curves are BEA predictions. Filled data points are experimental values for abraded glass (from Qasim et al.¹⁷). Arrows indicate unstable crack growth regions. The dashed curve in (d) is the BEA prediction for double radial crack.

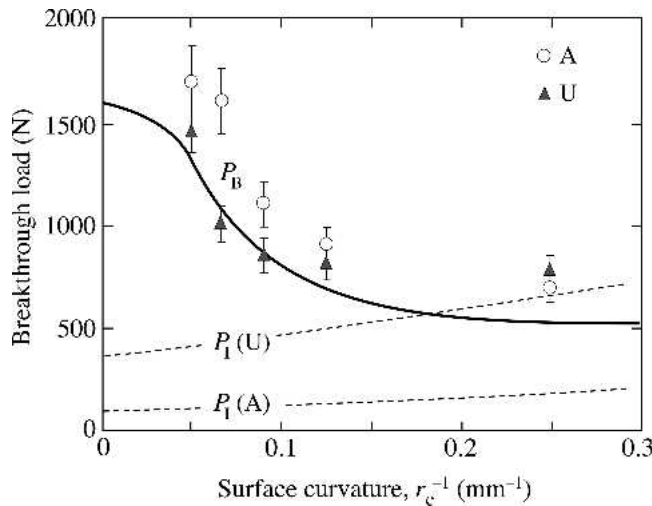


FIG. 9. Critical load P_B for breakthrough versus plate curvature r_c^{-1} , for glass/epoxy bilayers, $d = 1$ mm. The solid curve is BEA prediction. Data points are experimental values (mean and standard deviation) for abraded (A) and unabraded (U) glass, from Qasim et al.¹⁷ Dashed curves are corresponding smoothed data fits for initiation load P_I , also from Qasim et al.¹⁷

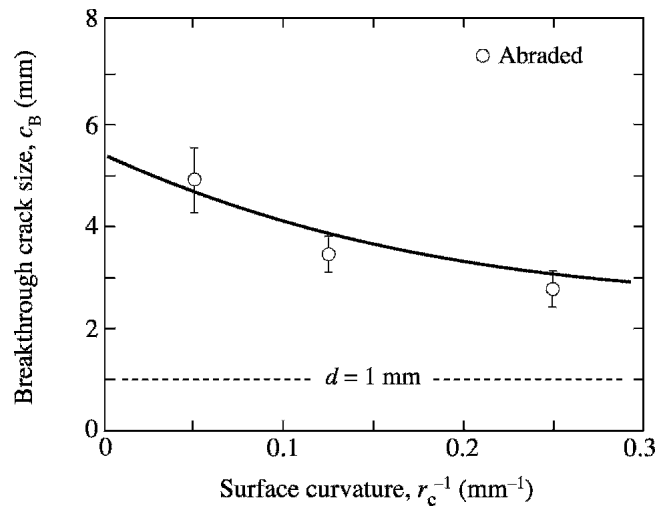


FIG. 10. Crack size c_B for radial crack breakthrough as function of curvature r_c^{-1} , for glass/epoxy, $d = 1$ mm. Data taken from Fig. 8: symbols are experimental values (mean and standard deviation); solid curve is smoothed curve through BEA maxima.

experimental values for glass with abraded and unabraded undersurfaces.¹⁷ (The lower dashed curves in Fig. 9 are critical loads P_I for crack initiation; see Sec. IV.) Both P_B and c_B diminish monotonically with increasing curvature, and are independent of starting flaw state. The basic experimental trends are reproduced by the calculated curves; however, the predictions for P_B lie

somewhat below the data, thereby providing only lower bounds for the failure condition.

Part of the reason for the numerical differences in Figs. 8–10 may lie in the oversimplistic assumption of a single radial crack in our first round of calculations. In reality, several such radial cracks form at regular angles to each other, with mutual interactions. To investigate this potential effect, repeat computations were performed with two mutually orthogonal radial cracks for the case

$r_c = 4$ mm. The results are included as the dashed curve in Fig. 8d. This curve lies a little closer to the experimental data, suggesting that computations for systems with multiple cracks might improve numerical agreement even more.

III. GENERALIZED FRACTURE MECHANICS

The BEA computations in the previous section considered the mechanics of radial fracture for one particular bilayer, glass of fixed thickness on an epoxy support base. Now we seek to extend the analysis to include any brittle coating of any thickness on any compliant base. We begin by recalling that the crack profiles in Fig. 5 reflect contours of tensile hoop stress, independent of coating thickness d .¹² It has been demonstrated that the tensile stress contours are insensitive to coating/substrate modulus ratio E_c/E_s , so that the crack profiles in Fig. 5 should be relatively material independent.¹² Thus, there is a certain universality in the crack geometry that allows us to generalize the fracture mechanics.

Accordingly, we may expect the stress-intensity factor for a radial crack of base radius c to assume the general form

$$K = \psi \sigma_0 c^{1/2} I(c/d) \quad , \quad (1)$$

where ψ is a dimensionless constant of value close to unity, σ_0 is the maximum (pre-crack) stress at the lower surface of the flexing brittle layer, and $I(c/d)$ is a dimensionless function of c/d .¹² The stress term has been shown to have the form

$$\sigma_0 = (P/Bd^2) \log(E_c/E_s) \quad , \quad (2)$$

where B is a dimensionless coefficient.⁷ It has further been demonstrated that σ_0 is virtually independent of surface curvature.¹⁷ The function $I(c/d)$ has a universal maximum value $I = 1$ at $c/d \ll 1$; and, because it is determined by the tensile stress distribution within the brittle layer, is relatively insensitive to material variation over the remainder of the c/d range.¹² However, $I(c/d)$ is expected to vary strongly with layer curvature to account for the different failure conditions at different r_c .¹⁷

Combining Eq. (1) and (2) then yields the generalized stress-intensity factor

$$K(c/d) = (\psi P/Bd^{3/2}) F(c/d) \log(E_c/E_s) \quad , \quad (3)$$

with $F(c/d) = (c/d)^{1/2} I(c/d)$. Thus the quantity $Kd^{3/2}/P \log(E_c/E_s)$ should be near-universal for any given c/d and material combination. Figure 11 is a plot of this quantity as a function of c/d for each r_c/d^{-1} . Stability conditions correspond to those apparent in Fig. 8: branches with $dK/dc < 0$ are stable; those with $dK/dc > 0$ are unstable. The function for the flat surface has only one unstable branch at small c/d and one stable branch

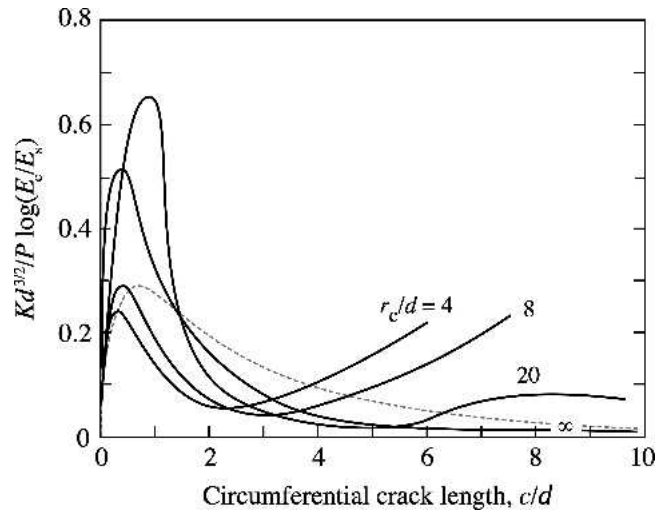


FIG. 11. Plot of $Kd^{3/2}/P \log(E_c/E_s)$ versus c/d for different curvatures r_c/d . Note different stability branches. Reference curve for infinite r_c/d (flat) has only one unstable and one stable branch. Curve for finite r_c/d (beyond some minimum value) has additional unstable branch in long-crack region, corresponding to failure. Light dashed curve is comparative estimate from analytical $K(c/d)$ expression for flat surfaces.¹²

at large c/d . For this special case, an earlier function based on an analytical estimation of $I(c/d)$ for flat surfaces with geometrically invariant half-penny cracks, using $B = 1.35$ and $\psi = 0.65$, is included as the light dashed curve in Fig. 11.¹² The functions for curved surfaces show an extra unstable branch at large c/d , corresponding to “failure” where the crack runs unimpeded to the specimen edge. Note how the breakthrough crack size c_B/d corresponding to the minima in these functions diminishes with increasing curvature $(r_c/d)^{-1}$. For cracks subject to equilibrium extension at $K = K_c$, we may use Eq. (3) to obtain a general expression for the breakthrough load $P = P_B$ at $c = c_B$:

$$P_B = (B/\psi F_B) K_c d^{3/2} / \log(E_c/E_s) \quad , \quad (4)$$

where $F_B = F(c_B/d)$ is a constant for any given curvature. The dependence of the critical conditions on material properties and layer thickness is now apparent.

IV. DISCUSSION

In this study, we have used boundary element analysis to determine the evolution of radial cracks in convex brittle coating layers on compliant substrates. The calculations are made on a model test system, 1-mm-thick glass of prescribed curvature on epoxy, and compared with corresponding available experimental data. As indicated in Sec. I., such a system has implications concerning the response to contact loading for a variety of layer systems, most notably dental crowns. The analysis accounts for various observed stages in the crack

growth: unstable pop-in from a subsurface flaw at a critical initiation load, arrest and stable extension with increasing applied load, breakthrough at the top surface, and unstable propagation to failure at the specimen edges. While increasing surface curvature of the brittle layer has little effect on the critical load to initiate the radial cracks, it strongly diminishes the critical load to final failure, i.e., the breakthrough load required to propagate the cracks to the specimen edges.

In the second part of this study, a generalized stress-intensity factor function $K(c/d)$ has been derived [Eq. (3)]. This formalism provides a basis for predicting failure load P_B under equilibrium conditions of crack growth, i.e., at $K = K_c$ [Eq. (4)]. The $K(c/d)$ function has explicit dependence on material properties (moduli E_c and E_s , toughness K_c) and layer thickness, and is expected to be near-universal for any convex curved surface. Whereas our BEA calculations are made specifically for glass of a specific thickness $d = 1$ mm on epoxy, Eq. (4) can be used to predict P_B for any monolithic ceramic material of any thickness on any substrate. It can be seen from Eq. (4) that higher resistance to failure requires brittle layer materials with higher E_c , K_c , and d , and substrates with lower E_s .

It is of interest to compare relations for the equilibrium critical load P_B for breakthrough [Eq. (4)] with the corresponding load P_I for initiation documented in earlier studies^{7,9,11}

$$P_I = B\sigma_F d^2 / \log(E_c/E_s) \quad (\text{initiation}) \quad , \quad (5a)$$

$$P_B = (B/\psi F_B) K_c d^{3/2} / \log(E_c/E_s) \quad (\text{breakthrough}) \quad , \quad (5b)$$

where σ_F is the strength of the brittle material. The load P_B can be substantially higher than P_I , so there is an inbuilt damage tolerance. The appearance of strength in Eq. (5a) in place of toughness in Eq. (5b) reflects a basic difference in the instability condition: initiation occurs at a critical stress from a pre-existing flaw, the scale of which is independent of specimen dimension; breakthrough occurs when the size of a well-developed crack reaches some critical value of c_B/d , independent of flaw size. This basic difference in instability condition is apparent in Fig. 9, which includes $P_I(r_c^{-1})$ functions for abraded and unabraded glass surfaces (dashed curves) from our preceding study.¹⁷ The ratio P_B/P_I decreases with increasing r_c^{-1} , highlighting a diminishing crack containment capacity in structures with greater curvature; indeed, the P_I curve for unabraded glass surfaces crosses the (flaw-independent) P_B curve, indicating that crack initiation in highly curved surfaces will take the system directly to failure.

An appeal of the $K(c/d)$ formulation of Eq. (3), quite apart from its universal applicability to different material

systems and different layer thicknesses, is its independence of a crack growth condition. Imposing $K = K_c$, as in the derivation of Eq. (4), yields a relation for failure under equilibrium conditions of extension. We could equally well impose a crack velocity relation, $v = v(K)$, to determine a relation for failure under kinetic conditions of extension, including cyclic loading (fatigue). Integration of the crack velocity function over its path to first instability has previously been performed to determine an explicit time-dependent relation for the initiation load $P_I(t)$.²⁸ Because the function $F(c/d)$ in Eq. (3) is not available in closed form, an analogous derivation of a time-dependent relation for failure $P_B(t)$ would require the integration to be performed numerically.

Implicit in the present study is the assumption that the contact radius at the interface between indenter and top surface of the brittle layer remains small relative to the specimen thickness, so that the stresses at the bottom surface of the brittle layer scale linearly with applied load. This was the case for the calculations in Sec. II. Such an assumption can become invalid for large indenters on thin layers, i.e., small d/r , leading to changes in the underlying mechanics and even in the mode of fracture.²⁹

Finally, as alluded to in Sec. I, top-surface fracture and deformation modes can occur and even dominate under different conditions, especially in thicker brittle layers and smaller indenters, i.e., large d/r .^{5,7,9,11,30} A full description of the competition between different damage modes could be a fruitful area of research in brittle coating technology.

ACKNOWLEDGMENTS

The authors gratefully acknowledge useful discussions with Xioazhi Hu and Chris Ford (University of Western Australia). This work was supported by a grant from the Australian Research Council and the United States National Institute of Dental and Craniofacial Research (PO1 DE10976).

Information of product names and suppliers in this paper is not to imply endorsement by the National Institute of Standards and Technology.

REFERENCES

1. A.W. Eberhardt, J.L. Lewis, and L.M. Keer: Normal contact of elastic spheres with two elastic layers as a model of joint articulation. *ASME J. Biomed. Eng.* **113**, 410 (1991).
2. D.F. Diao, K. Kato, and K. Hokkirigawa: Fracture mechanisms of ceramic coatings in indentation. *Trans. ASME J. Tribol.* **116**, 860 (1994).
3. L. An, H.M. Chan, N.P. Padture, and B.R. Lawn: Damage-resistant alumina-based layer composites. *J. Mater. Res.* **11**, 204 (1996).
4. T.J. Lardner, J.E. Ritter, and G-Q. Zhu: Spherical indentation and fracture of glass plates. *J. Am. Ceram. Soc.* **80**, 1851 (1997).

5. H. Chai, B.R. Lawn, and S. Wuttiphphan: Fracture modes in brittle coatings with large interlayer modulus mismatch. *J. Mater. Res.* **14**, 3805 (1999).
6. B.R. Lawn, K.S. Lee, H. Chai, A. Pajares, D.K. Kim, S. Wuttiphphan, I.M. Peterson, and X. Hu: Damage-resistant brittle coatings. *Adv. Eng. Mater.* **2**, 745 (2000).
7. Y-W. Rhee, H-W. Kim, Y. Deng, and B.R. Lawn: Contact-induced damage in ceramic coatings on compliant substrates: Fracture mechanics and design. *J. Am. Ceram. Soc.* **84**, 1066 (2001).
8. H. Zhao, X. Hu, M.B. Bush, and B.R. Lawn: Cracking of porcelain coatings bonded to metal substrates of different modulus and hardness. *J. Mater. Res.* **16**, 1471 (2001).
9. Y. Deng, B.R. Lawn, and I.K. Lloyd: Characterization of damage modes in dental ceramic bilayer structures. *J. Biomed. Mater. Res.* **63B**, 137 (2002).
10. H. Chai: Fracture mechanics analysis of thin coatings under spherical indentation. *Int. J. Fract.* **119**, 263 (2003).
11. B.R. Lawn, A. Pajares, Y. Zhang, Y. Deng, M. Polack, I.K. Lloyd, E.D. Rekow, and V.P. Thompson: Materials design in the performance of all-ceramic crowns. *Biomaterials* **25**, 2885 (2004).
12. H-W. Kim, Y. Deng, P. Miranda, A. Pajares, D.K. Kim, H-E. Kim, and B.R. Lawn: Effect of flaw state on the strength of brittle coatings on soft substrates. *J. Am. Ceram. Soc.* **84**, 2377 (2001).
13. J.R. Kelly: Clinically relevant approach to failure testing of all-ceramic restorations. *J. Prosthet. Dent.* **81**, 652 (1999).
14. B.R. Lawn, Y. Deng, and V.P. Thompson: Use of contact testing in the characterization and design of all-ceramic crown-like layer structures: A review. *J. Prosthet. Dent.* **86**, 495 (2001).
15. G. Willmann: Ceramic femoral heads for total hip arthroplasty. *Adv. Eng. Mater.* **2**, 114 (2000).
16. G. Willmann: Improving bearing surfaces of artificial joints. *Adv. Eng. Mater.* **3**, 135 (2001).
17. T. Qasim, M.B. Bush, X. Hu, and B.R. Lawn: Contact damage in brittle coating layers: influence of surface curvature. *J. Biomed. Mater. Res.* **3**, 179 (2005).
18. T. Qasim, C. Ford, M.B. Bush, X. Hu, and B.R. Lawn: Effect of off-axis concentrated loading on failure of curved brittle layer structures. *J. Biomed. Mater. Res. B* (in press).
19. B.R. Lawn: Indentation of ceramics with spheres: A century after Hertz. *J. Am. Ceram. Soc.* **81**, 1977 (1998).
20. B.R. Lawn: Ceramic-based layer structures for biomechanical applications. *Curr. Opin. Solid State Mater. Sci.* **6**, 229 (2002).
21. Y. Cao: Three-dimensional finite element modeling of subsurface median crack in trilayer sandwiches due to contact loading. *Eng. Fract. Mech.* **69**, 729 (2002).
22. M.B. Bush: Prediction of crack trajectory by the boundary element method. *Struct. Eng. Mech.* **7**, 575 (1999).
23. M. Rudas, M.B. Bush, and I.E. Reimanis: The kinking behaviour of a bimaterial interface crack under indentation loading. *Eng. Anal. Bound. Elem.* **28**, 1455 (2004).
24. D.P. Rooke and D.J. Cartright: *Compendium of Stress Intensity Factors* (Hillingdon Press, Uxbridge, Middlesex, U.K., 1976).
25. I.M. Peterson, A. Pajares, B.R. Lawn, V.P. Thompson, and E.D. Rekow: Mechanical characterization of dental ceramics using Hertzian contacts. *J. Dent. Res.* **77**, 589 (1998).
26. K.K. Ray and A.K. Dutta: Comparative study on indentation fracture toughness evaluations of soda-lime glass. *Brit. Ceram. Trans.* **98**, 165 (1999).
27. Y-W. Rhee, H-W. Kim, Y. Deng, and B.R. Lawn: Brittle fracture versus quasiplasticity in ceramics: A simple predictive index. *J. Am. Ceram. Soc.* **84**, 561 (2001).
28. C-S. Lee, D.K. Kim, J. Sanchez, P. Miranda, A. Pajares, and B.R. Lawn: Rate effects in critical loads for radial cracking in ceramic coatings. *J. Am. Ceram. Soc.* **85**, 2019 (2002).
29. H. Chai and B.R. Lawn: Fracture mode transitions in brittle coating layers on compliant substrates as a function of thickness. *J. Mater. Res.* **19**, 1752 (2004).
30. Y. Zhang, S. Bhowmick, and B.R. Lawn: Competing fracture modes in brittle materials subject to concentrated cyclic loading in liquid environments: Bilayer structures. (in press).